Experimental study of collisional granular flows down an inclined plane

By EMMANUEL AZANZA, FRANÇOIS CHEVOIR†
AND PASCAL MOUCHERONT

Laboratoire des Matériaux et Structures du Génie Civil, UMR LCPC-CNRS,
2 allée Kepler, 77 420 Champs sur Marne, France

The collisional flow of a slightly inelastic granular material down a rough inclined plane is usually described by kinetic theories. We present an experimental study aimed at analysing the assumptions and the quantitative predictions of such theories. A two-dimensional channel coupled to a model granular material and image analysis allow detailed and complete measurement of the kinematics and structure of the flows. We determine the range of inclination and particle flux for which the flow is stationary and uniform. The characteristic profiles of solid fraction, mean velocity and granular temperature are systematically measured. Both the true collisional and the dilute kinetic regimes are examined. We show that a quasi-hydrodynamic description of these regimes seems relevant, and that the pressure and the viscosity terms are in good qualitative agreement with the prediction of the kinetic theory. The profiles are well described by the kinetic theory near the top of the flow, at low solid fraction. Conversely there are large discrepancies near the rough plane, where the material is structured in layers.

1. Introduction

The formulation of constitutive laws for a granular flow is still an active field of research. According to the nature of the flow regime (frictional or collisional), several formulations have been suggested. If the granular medium is dense and slowly sheared, the particles have persistent contacts and dissipate energy by friction. The forces between particles have a static origin and the constitutive law is 'plastic'-like (Brown & Richards 1970; Nedderman 1992). On the other hand, if the flow is dilute and highly sheared, the particles interact collisionally, which dissipates a part of their kinetic energy. In this case, the constitutive laws may be deduced from a microstructural approach, similar to the kinetic theory for dense gas (Campbell 1990).

During the last two decades kinetic theory has been continually improved (Savage & Jeffrey 1981; Jenkins & Savage 1983; Lun *et al.* 1984; Jenkins & Richman 1985; Lun 1991). This theory has the great advantage of linking the macroscopic behaviour of the granular medium to local interactions between particles. Inside a real granular medium, those local interactions are very complex. That is why the theoretical models consider model granular media, usually spheres or disks with uniform diameters. In this case, it is possible to describe the interactions of contact between the particles by simple models. When a granular medium is highly sheared, the collisions generate a fluctuating component of the velocity of the particles, measured by the granular

† Author to whom correspondence should be addressed: e-mail: chevoir@lcpc.fr.

temperature. But unlike a gas, inelastic collisions between the particles have a direct effect on the value of the granular temperature.

The kinetic theory supplies a unique formalism to derive both the balance laws and the constitutive relations for the collisional, slightly inelastic granular flows. The expression for the stress tensor depends on the solid fraction, the granular temperature and their gradients (Lun *et al.* 1984; Jenkins & Richman 1985), in accordance with the arguments of Bagnold (1954). Besides, an equation for energy, representing the balance of the modes of production, conduction and dissipation of granular temperature, has been established (Jenkins & Savage 1983). It involves the flux of fluctuation kinetic energy and the rate of energy dissipation.

In order to examine the validity of this theory, several numerical simulations have been performed using the molecular dynamics method. However, those simulations essentially deal with uniform plane shear geometry; their results cannot be directly generalized to more complex geometries. They have improved our knowledge of the dependence of the stress tensor on solid fraction and granular temperature (Campbell & Brennen 1985; Campbell & Gong 1986; Walton & Braun 1986*a*; Lun & Bent 1994). They have also helped to highlight the importance of the anisotropy of granular temperature, which was not initially taken into account in the theories (Campbell & Brennen 1985; Campbell & Gong 1986; Walton & Braun 1986*b*), and specify the effects of particle rotation (Campbell 1989), boundary conditions (Campbell 1993; Louge 1994), and the development of structure in granular media (Campbell & Brennen 1985; Campbell 1986; Zhang & Campbell 1992; Savage & Dai 1993).

Experimental studies devoted to the collisional regime have been less numerous than numerical studies. The wide heterogeneity of experimental set-ups and measurement techniques complicates the interpretation of the results (Ishida & Shirai 1979; Savage 1979; Johnson, Nott & Jackson 1990; Ahn, Brennen & Sabersky 1991). Moreover, the development of microstructural theories, like kinetic theory, has represented a new challenge to the experimentalists. The main assumptions on which they are founded can be proved only by a detailed study of the kinematics and structure of the flows. Unfortunately, the current state of experimental technique does not allow us to measure the contact forces between the particles, limiting our knowledge of the energy dissipation features inside the flows. Simply measuring the granular temperature, a basic quantity in the collisional regime, raises a big problem. It is impossible to determine the particle velocity inside a three-dimensional flow because inserting a probe seriously disturbs the measurement. For this reason, the measurements are usually performed at the wall, like in the study by Ahn *et al.* (1991). But most of the recent experimental studies do not present any measurements of granular temperature. To avoid the experimental difficulties encountered in the case of a three-dimensional flow, Drake (1991) proposed using a two-dimensional geometry where the particles are confined to just one layer. This geometry is well suited to an analysis of the microstructure of the flows. In this way, he was able to measure the kinematics of the flows, filming the particle motion with a high speed camera, and presented profiles of solid fraction, mean velocity and granular temperature. However, no detailed comparison between experimental results and kinetic theory predictions was carried out.

The aim of this article is to test some aspects of the kinetic theory of granular materials with an experiment involving granular flows down an inclined plane. Our approach is very similar to Drake's: we have built a two-dimensional channel and used a rapid visualization technique. We have developed automatic analysis of the pictures, which gives rapid quantitative measurements and permits the study of very varied

Diameter, D (mm)	3
Mass density, ρ_p (kg m^{-3})	7.8×10^3
Normal restitution coefficient, e	0.95
Friction coefficient, μ	0.2

TABLE 1. Geometrical and physical properties of the steel beads.

dynamical phenomena. The profiles of solid fraction, mean velocity and granular temperature have been systematically measured, and compared with the predictions of the kinetic theory. Complementary results may be found in Azanza, Chevoir & Moucheront (1997) and Azanza (1998).

Section 2 of this paper is devoted to a detailed presentation of the experimental set-up. Section 3 explains the predictions of the kinetic theory for a granular flow down an inclined plane, and especially the stress tensor expression. Sections 4 and 5 present comparisons between experimental results and theoretical predictions for the collisional and the dilute kinetic regimes.

2. Experimental set-up

In this Section, the experimental techniques will be presented. In particular, the order of magnitude of the extraneous effects that may disturb the interpretation of experimental results, such as the sidewall friction, will be examined.

2.1. *Description*

2.1.1. *Characterization of the granular medium*

The experiments were carried out with monodisperse metallic beads whose diameter D is equal to 3 mm. The tolerances on the diameter and on sphericity are very good because these beads are used as ball bearings in industry. In order to study the collisional regime and discuss the validity of kinetic theories, we have used steel beads, i.e. a low dissipative material which favours the collisional regime. The bead properties are shown in table 1. The restitution coefficient of the bead has been measured on the one hand from the study of the impacts of the beads on a marble table and on the other hand from binary collisions between beads inside the channel. In both cases, the restitution coefficient is equal to 0.95 ± 0.03 and remains constant throughout the velocity range considered (velocity less than 1 m s^{-1}, and larger than a few cm s^{-1}). The friction coefficient has not been measured, and its value has been taken from Bowden & Tabor (1950).

2.1.2. *The channel*

The channel consists of two glass walls, 2 m long, 20 cm deep and 1 cm thick (figure 1). The gap between the walls is regulated with precision wedges in order to confine the material to only one bead layer. This gap must be slightly larger than the bead diameter to avoid any locking, but small enough to preserve the two-dimensional feature of the experiment. The inclination range (θ) of the channel varies from 0° to 40° with respect to the horizontal. A two-dimensional hopper feeds the channel. The feeding particle flux (Q) is controlled by changing the aperture and its value cannot exceed 1800 particles per second. The tank is situated 17 cm above the channel bed so that the particles acquire initial velocity. The beads accelerate on a smooth bottom
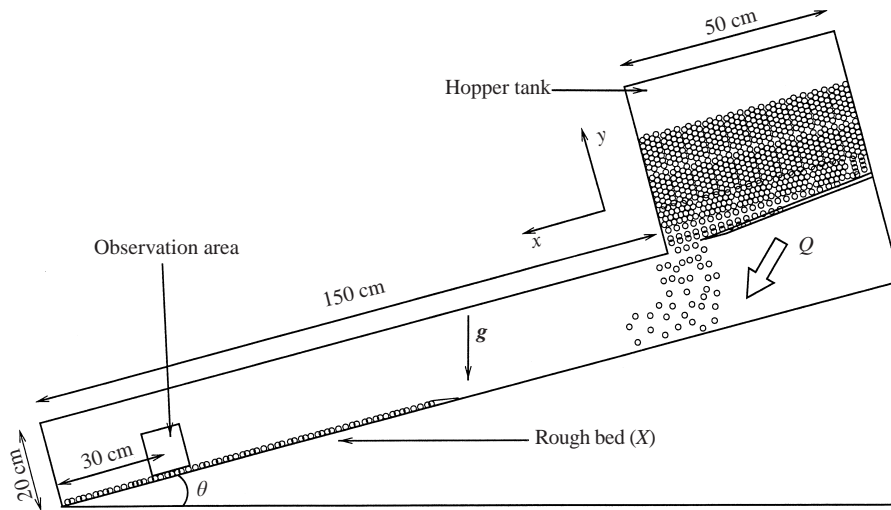
FIGURE 1. Two-dimensional channel.

about 50 cm long and then bump onto a rough bed which disorganizes them and slows them down.

Two kinds of rough beds have been used. The first one is made up of beads similar to the flowing ones. They are firmly stuck on a steel bar in a layer of Araldite glue which comes up to half their height. Once dry, this glue is very hard and the beads are well fixed. The spacing between the beads is not constant; it varies from 0 to 1.7 radii in order to make sure that a bead in the flow cannot touch the glue layer. This rough bed is characterized by an effective bed roughness X (defined as the ratio of the length of the stuck beads placed end-to-end to the total length of the bed) of 0.78, equivalent to a mean distance between the beads of 0.29 diameter. The second rough bed was obtained by machining a steel bar to a jagged profile. The characteristic size of the roughness is not constant but its order of magnitude always remains slightly larger than a bead diameter.

2.1.3. *Image acquisition*

The flows are filmed with a high speed digital 8 bit camera (Dalsa CAD4), at a rate of 230 images per second. The filmed area is located about 30 cm upstream from the channel outlet and its size is about 4 cm. It is lit by a stroboscope synchronized with the camera clock, whose flashes have a mean duration of 10 μs in order to obtain sharp images, without the fuzziness due to the particle motion. To obtain very contrasted images, the stroboscope is placed just in front of the camera (ombroscopy). Moreover, a light diffuser located on the glass wall of the channel makes the lighting uniform and improves the quality of the images. The images from the camera are stored temporarily in the RAM of the computer via a video card linked to a rapid acquisition module (AMDIG, 16 MHz). The digital film, corresponding to 6 s of flow, is then stored in the hard disk.

2.1.4. *Processing of digital images*

The digital images are then analysed to obtain the main quantities of the flow, such as the solid fraction v, mean velocity $\boldsymbol{u}$ and granular temperature T, defined as $T = 1/d\langle C^2 \rangle$, with $\boldsymbol{C}$ being the fluctuating component of the velocity and d the
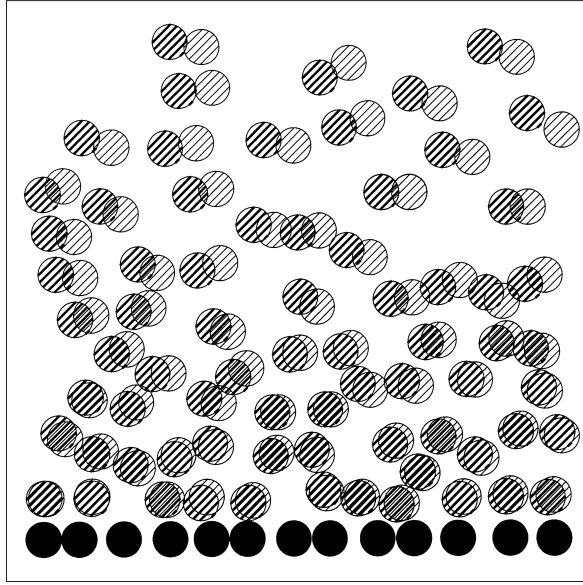
FIGURE 2. Picture of the flow with the double-flash lighting method.

dimension of the space. Introducing characteristic length D, velocity $(gD\cos\theta)^{1/2}$ (see §3) and time $(D/g)^{1/2}$, we will often use dimensionless quantities in the following, indicated by the *:

$$y^* = y/D, \tag{2.1}$$

$$u^* = u/(gD\cos\theta)^{1/2}, \tag{2.2}$$

$$T^* = T/gD\cos\theta. \tag{2.3}$$

The image processing method depends on the measurement of the temperature and requires the greatest care. Measuring granular temperature involves knowing the instantaneous velocity of the particles, i.e. the velocity between two collisions. This velocity is calculated from successive particle positions. In order to make sure that there is no collision between these two positions, we have to take care that the sampling time of the positions τ_s is smaller than the mean time between two successive collisions τ_{col}. The sampling time τ_s is given by the acquisition rate of the camera and rises to 4.3×10^{-3} s. The mean time between two successive collisions is $\tau_{col} = \ell/T^{1/2}$, where ℓ is the mean free path of the particles. Consequently, the largest granular temperature T_l which can be measured is $T_l = (\ell/\tau_s)^2$. In fully developed collisional flows, we will see in §4 that the order of magnitude of the dimensionless granular temperature is about 1. In such flows, the mean free path is well estimated by the mean distance between the particles

$$\ell = D\left((v_m/v)^{1/2} - 1\right), \tag{2.4}$$

with v_m the random close packing solid fraction ($v_m = 0.82$ in two dimensions).

As a result, the measurement of the granular temperature is no longer valid for solid fraction larger than 0.5. In order to ensure accurate measurement of the granular temperature at solid fractions as high as 0.7, the sampling time τ_s must be reduced by a factor 4 (an alternative would be to use larger particles). We modified the working of the stroboscope so that it delivers two successive flashes instead of one during the
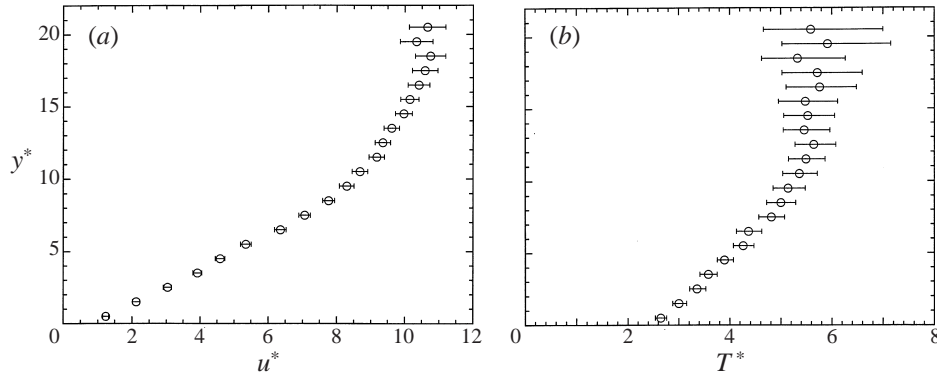
FIGURE 3. Experimental errors: (a) average velocity u^*, (b) granular temperature T^* ($\theta = 23°$, $Q \simeq 1100$ particles per second, stuck-bead bed roughness).

integration time of the camera. The two successive positions of each particle thus appear on the same image (figure 2). These positions are more or less close and may partially overlap according to the time interval between the two flashes. Since the first and second flashes have different intensities, the direction of the particle displacement is known. The double flash lighting method is thus convenient for measuring granular temperature in the collisional flows.

Thanks to double flash images, it is easy to find the position and the velocity of each particle by image processing. Note that it is not possible to measure the particle rotation. A multiple threshold is applied to separate the successive positions of the particles. Since the two flashes have different intensities, these positions exhibit distinct grey levels and the overlapped areas appear deep grey. Then it is possible to reconstitute two binary images, the first one with the initial positions of the beads (deep and median grey levels) and the second one with the final positions (light and median grey levels). The centre of mass of each particle is then calculated. The precision on the determination of the centre of mass depends on the size of the particle diameter in pixels. Since this diameter is about 20 pixels, the error made is less than one pixel. Depending on camera resolution (256×256 pixels), the size of the recorded images is about 13 bead diameters. The small displacement of the beads between two flashes makes it possible to calculate their velocity without ambiguity. However, the beads which move in or out of the filmed area have an undetermined velocity. That is why a margin of one diameter is systematically applied on the sides of the images to exclude these questionable cases.

From the bead velocities, the mean kinetic energy of the particles is calculated and the analysis of its variation during the 6 s of the film allows us to define the range of stationary flow, if it exists. We consider that the flow is in a steady state if the variations of the kinetic energy do not exceed 10% of its mean value. With a view to determining the profiles of the mean quantities describing the flow in the direction normal to the channel bed, namely the solid fraction, mean velocity and granular temperature, the images are divided into layers 1 bead diameter wide, parallel to the bed channel, inside which the averages are calculated. The solid fraction is defined as the ratio of the apparent bead surface inside the layer to the total layer surface. The velocity and granular temperature are calculated with the beads whose centre of mass is inside the layer. These quantities are also averaged over time during the maximum time of steady-state flow (this time is at least 3 s). Each measurement set thus

corresponds to more than 1000 different positions. Figure 3 shows the experimental uncertainties, associated with image processing and statistical processing of data. This last error is the most significant one. It is negligible for the solid fraction. Conversely, it affects the mean velocity and granular temperature profiles to a greater extent. The error in the velocity is less than 5%, except in the upper part of the flows where it reaches 10%. As for the error on the granular temperature, it is 10% higher at the channel bed and reaches 35% when the solid fraction is very low and the particle number on which the average is performed is less than 500. The error bars will not be shown any more in the following.

This averaging process is only valid if the flows are uniform (or fully developed) in the direction parallel to the plane. This uniformity is checked by filming areas situated at different distances upstream from the channel outlet and comparing the profiles with the ones determined in the region situated at 30 cm from the outlet. The flows are considered to be uniform when the discrepancies between the profiles are restricted to a few percent. In the following, this condition is checked in regions located less than 50 cm upstream of the channel outlet.

2.2. Extraneous effects

In addition to contact interaction (friction and inelastic collisions), the particles can undergo aerodynamic and electrostatic effects. Besides, the walls which confine the material may generate some perturbations. Most microstructural theories do not take these effects into account. It is therefore essential to estimate their order of magnitude before comparing the experimental results with the predictions of the theories.

2.2.1. *Aerodynamic and electrostatic effects*

Let us estimate the order of magnitude of the aerodynamic force F_a exerted on the beads by the air and compare it to the driving force of the particles, their weight P. Consider an unfavourable case in which the beads move through immobile air with a velocity V equal to 1 m s^{-1}. The Reynolds number is of the order of 100, so that the viscous friction force expression, assuming that the particles are isolated, is $F_a = \frac{1}{8}C_v\pi\rho_f D^2 V^2$, with C_v a characteristic coefficient depending on the material shape whose value is close to 0.5 in this case, and ρ_f the mass density of the air. The non-dimensional ratio R_a, defined

$$R_a = \frac{P}{F_a} = \frac{4D\rho_p g}{3C_v\rho_f V^2}, \tag{2.5}$$

being equal to 470, the viscous forces exerted on the beads are negligible with regard to the driving force of the particles. Moreover the hindering effect of the other particles should lower the viscous force, so that this estimation is an over-estimate.

In addition to aerodynamic effects, the beads can undergo electrostatic effects. The collisions between the steel particles and the glass walls induce electric charge transfers which may accumulate locally on the surfaces. The order of magnitude of the charge transferred in such collision is $Q_c = 10^{-13}$ C (Lowell & Rose-Innes 1980). From Appendix A, the frequency of collisions with the wall is of the order of $(g/D)^{1/2}$ (around 50 s^{-1}). Consequently, during an experimental flow which lasts around 10 s, the maximum charge which can accumulate on a bead (Q_m) is less than 10^{-10} C. Moreover, this electric charge does not accumulate on the bead but diffuses inside the granular flow because of the collisions between the metallic particles, and disappears at the metallic bed. This diffusion process is regulated by two mean free paths. The first one (ℓ_w) is associated with the collisions with the wall (of the order

of D), and the second one (ℓ) is associated with the collisions between grains, and quantified by (2.4). Then in a layer of height H, the maximum charge is of the order $Q_m = Q_c \left(H^2/\ell\,\ell_w \right)$. For $H = 10D$ and a solid fraction less than 0.7, this gives roughly the same estimation as before. Those two values are smaller than the maximum electrostatic charge estimated from the ionization field of the air ($3\ \mathrm{MV^{-1}}$), which rises to 10^{-9} C for beads 3 mm in diameter.

Using Coulomb's law, let us now estimate the force of repulsion F_e which acts between two beads carrying the same charge Q_m separated by a distance of about one diameter: $F_e = Q_m^2/4\pi\epsilon_0 D^2$, with $\epsilon_0 = 8.85\,10^{-12}\ \mathrm{F\,m^{-1}}$ the permeability of a vacuum (the correction due to influence effects is less than 4%). The comparison with the weight defines the non-dimensional ratio R_e

$$R_e = \frac{P}{F_e} = \frac{2\pi^2\epsilon_0 D^5 \rho_p g}{3Q_m^2}. \tag{2.6}$$

The previous estimation gives a ratio R_e of the order of 100. As a matter of fact, we have never noticed any macroscopic manifestations of electrostatic effects during the experiments. In the following, we will assume that the aerodynamic and electrostatic forces do not disturb the flows and we systematically neglect them.

2.2.2. *Wall influence*

Few studies have been devoted to the influence of the walls on granular flow in a channel (Savage 1979; Drake 1991; Ahn *et al.* 1991; Hanes *et al.* 1997) even though the most commonly used experimental techniques do not allow measurements to be taken inside the material, because the insertion of a probe is a perturbation factor. The only information accessible is situated on the walls and cannot be interpreted before an estimation of generated perturbations.

We have focused special attention on the design of the channel in order to minimize this influence. A tightening system reduces the bending of the glass plates and improves their parallelism. Moreover, the glass planes present flatness characteristics higher than the average and their thickness (1 cm) contributes to their rigidity. The extra gap σ between the walls is controlled with precision metal bars and it is set to approximately 0.05 mm.

In fact, in our two-dimensional geometry, the beads do not flow strictly in a plane, they suffer off-centre collisions and collide with the walls.

Measuring the velocity before and after a collision, we first calculated the effective restitution coefficient between the particles themselves and between the particles and the rough bed for various extra gaps, and observed no appreciable variation.

However figure 4 shows a strong influence of the spacing on the profiles of solid fraction and velocity. For a given inclination of 21° and particle flux of 1400 particles per second, the extra gap between the walls was varied between $\sigma = 0.05$ mm and $\sigma = 0.2$ mm. The flows remain truly collisional, and no wedging effect is observed during the experiment. However, the larger the gap, the slower and denser is the flow. For extra gaps greater than 0.2 mm, the profiles are not shown since the flows stop. We made sure that the flows were reproducible.

In Appendix A we estimate the average friction force exerted by the walls on a bead

$$\boldsymbol{F}_f = m(1 + e_w)(1 + e)^2\,\mu_w\frac{\sigma}{D}gT^*\,\boldsymbol{t}, \tag{2.7}$$

where $\boldsymbol{t}$ is the unit vector pointing in the opposite direction to the mean velocity flow,
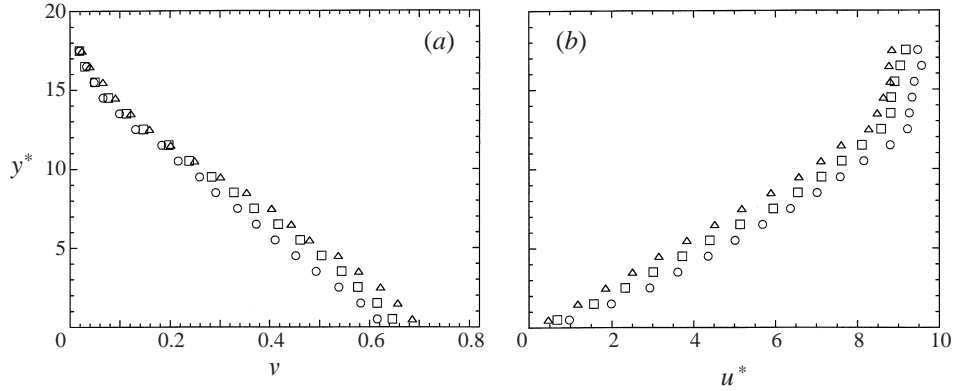
FIGURE 4. Influence of the spacing between the walls ($s = 0.05$ mm ($\bigcirc$), $s = 0.1$ mm ($\square$) and $s = 0.15$ mm ($\triangle$)): (*a*) profile of solid fraction v, (*b*) profile of velocity u^* ($\theta = 21°$, $Q \simeq 1400$ particles per second, stuck-bead bed roughness).

and e_w and μ_w are respectively the restitution coefficient between the beads and the glass walls and the friction coefficient at the wall. Consequently, we may define the effective gravity acting on the particles $\boldsymbol{g}^{eff} = \boldsymbol{g} + \boldsymbol{F}_f/m$, which makes an angle ψ with the vertical

$$\psi = (1 + e_w)(1 + e)^2 \mu_w \frac{s}{D} T^*. \tag{2.8}$$

Thus an increase in the extra gap corresponds to a reduction in the plane inclination. Taking $e = e_w = 0.95$, $\mu_w = 0.2$, $\sigma = 0.1$ mm, $D = 3$ mm and $T^* = 1$, we find an angle $\psi = 2.9°$.

This simple model may partly explain the order of magnitude of the observed variations of the solid fraction and velocity profiles.

3. Kinetic theory

Collisional flows are usually modelled with the kinetic theory (Campbell 1990). The great advantage of this theory is that it links the macroscopic behaviour of the granular medium with the particle-scale interactions between its constituents. From simple interaction models, an appropriate averaging processing gives access to the constitutive law.

Let us consider the two-dimensional problem of a set of identical disks (or spheres) of diameter D, mass density ρ_p and mass m, flowing down a plane inclined at an angle θ with respect to the horizontal. The particles are subjected to a driving force $\boldsymbol{F}$ associated with their weight $m\boldsymbol{g}$. We assume that the flows are steady state and uniform in the direction of the plane (Ox), so that the solid fraction v, the mean velocity in the direction of the flow u and the granular temperature T only depend on the height above the channel bed y. Following these assumptions, the momentum balance equation (projected along (Ox) and (Oy)) and the energy equation take the form (Ahn, Brennen & Sabersky 1992)

$$\rho_p v g \cos\theta + \frac{d\Sigma_{yy}}{dy} = 0, \tag{3.1}$$

$$\rho_p v g \sin\theta - \frac{d\Sigma_{xy}}{dy} = 0, \tag{3.2}$$

$$\Sigma_{xy}\frac{du}{dy} + \frac{dq_y}{dy} + \gamma = 0. \tag{3.3}$$

The continuity equation is automatically satisfied. Σ_{yy} and Σ_{xy} are respectively the normal and shear stress, q_y is the component normal to the plane of the flux of fluctuation kinetic energy and γ is the rate of energy dissipation. Their expressions depend on the details of the kinetic theory considered. In the following, we will consider the system of equations established by Jenkins & Richman (1985) to describe the dynamics of monodisperse, slightly inelastic and smooth disks (no rotation is considered). This theory makes the following assumptions:

collisions are binary and instantaneous;

the pre- and post-collision velocities of the particles are not correlated (molecular chaos);

the kinematic collision model is simple (Newton's coefficient of normal restitution);

the granular medium is close to equilibrium (the single-particle distribution function is quasi-Maxwellian);

the gradient of the main quantities is small;

the energy dissipated by collisions is small (the coefficient of normal restitution is close to 1 and the friction coefficient is negligible).

On the basis of these assumptions, the normal and shear stresses, the flux of fluctuation kinetic energy and the rate of energy dissipation are derived from Boltzmann's equation (Jenkins & Richman 1985):

$$\Sigma_{yy} = \rho_p f_1(v)T, \tag{3.4}$$

$$\Sigma_{xy} = \rho_p D f_2(v)T^{1/2}\frac{du}{dy}, \tag{3.5}$$

$$q_y = -\rho_p D\left(f_3(v)T^{1/2}\frac{dT}{dy} + f_4(v)T^{3/2}\frac{dv}{dy}\right), \tag{3.6}$$

$$\gamma = \frac{\rho_p}{D}f_5(v)T^{3/2}. \tag{3.7}$$

The functions $f_i(v)$ are given in Appendix B. They depend on the radial distribution function at contact $g_0(v)$, which is defined in Appendix C. By measuring the correlations of the positions in an assembly of particles, the radial distribution function quantifies the structure of a disordered medium. Its value at contact $g_0(v)$ is a measurement of the density of contacting particles in the assembly, and allows the calculation of the collision rate between the particles. For low solid fractions, g_0 tends to 1, it increases with the solid fraction, and diverges close to the maximum allowable solid fraction. In two-dimension geometry, an expression has been given by Verlet & Levesque (1982):

$$g_0^{VL}(v) = \frac{16 - 7v}{16(1-v)^2}. \tag{3.8}$$

The functions f_i and g_0 diverge when the solid fraction reaches 1, a value without physical meaning, instead of at the maximum packing value ($v_m = 0.82$). For this

reason, Ahn *et al.* (1992) used another expression for g_0 which diverges at v_m:

$$g_0^{v_m}(v) = \frac{1}{1 - (v/v_m)^{1/2}} \,.$$ (3.9)

On the other hand, these functions are finite in the neighbourhood of $v = 0$. As in a gas, the pressure, deduced from (3.4), is proportional to the temperature, and the viscosity, deduced from (3.5), is proportional to the square root of the temperature. The flux of fluctuation kinetic energy is the sum of a term similar to Fourier's law and a term which takes into account the solid fraction gradient (which has an uncertain physical origin). The normal and shear stresses and the flux of fluctuation kinetic energy are the sum of two terms:

a collisional contribution, which takes the transfer of momentum and fluctuant kinetic energy during collisions into account, and which is significant for high solid fractions;

a kinetic contribution, which takes the transfer of momentum and fluctuant kinetic energy transfer between two collisions into account, and which is significant for low solid fractions.

Let us write the balance equations (3.1), (3.2) and (3.3) in the way of Ahn *et al.* (1992). Combining (3.1) and (3.2) and assuming that the pressure and shear stress vanish at infinity, we obtain

$$\frac{\Sigma_{yy}}{\Sigma_{xy}} = -\tan\theta.$$ (3.10)

Using the expressions (3.4)–(3.7) for Σ_{yy}, Σ_{xy}, q_y and γ in (3.1), (3.3) and (3.10), and taking the non-dimensional form for y, u and T, (3.1) and (3.10) become

$$\frac{\mathrm{d}v}{\mathrm{d}y^*} = -\frac{1}{f_1' T^*}\left(v + f_1 \frac{\mathrm{d}T^*}{\mathrm{d}y^*}\right),$$ (3.11)

$$\frac{\mathrm{d}u^*}{\mathrm{d}y^*} = \tan\theta F(v) T^{*1/2},$$ (3.12)

with $F(v) = f_1/f_2$ and $f_1' = \mathrm{d}f_1/\mathrm{d}v$. Using the expressions $\mathrm{d}v/\mathrm{d}y^*$ and $\mathrm{d}u^*/\mathrm{d}y^*$ obtained in (3.11) and (3.12), the energy balance (3.3) becomes

$$\frac{\mathrm{d}^2 T^*}{\mathrm{d}y^{*2}} = F_1(v)\left[F_2(v)T^* + \frac{1}{T^*}\left(F_3(v)\left(\frac{\mathrm{d}T^*}{\mathrm{d}y^*}\right)^2 + F_4(v)\frac{\mathrm{d}T^*}{\mathrm{d}y^*} + F_5(v)\right)\right].$$ (3.13)

The functions F_i are the combination of the products of functions f_i with their derivatives. Their expressions are given in Appendix B.

The variations of the solid fraction and of the granular temperature are linked by the system (3.11) and (3.13). Equation (3.12) quantifies how the granular temperature is generated by the velocity gradient. If we put this relation in the expressions for pressure (3.4) and shear stress (3.5), we recognize the famous law established by Bagnold (1954), which states the dependence of the normal and shear stresses on the square of the velocity gradient. We emphasize that there are only two parameters in this model: the restitution coefficient e, and the radial distribution function at contact $g_0(v)$.
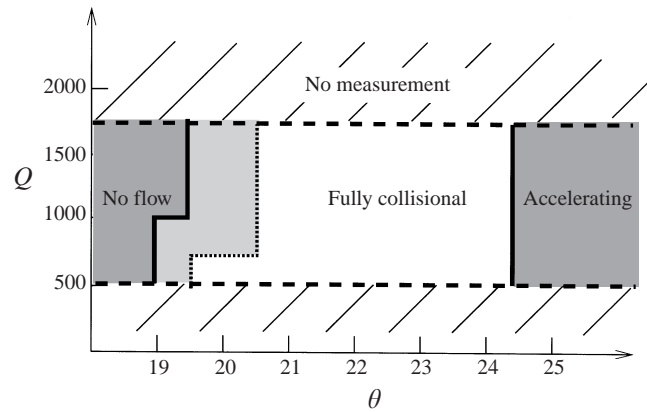
FIGURE 5. (Particle flux Q, inclination angle θ) diagram of stationary and uniform flow (stuck-bead bed roughness).

4. Collisional regime

4.1. *Experimental diagram and characteristic profiles*

Figure 5 shows a diagram of the flow on the stuck bead bed. The status of a flow (steady state, accelerating or stopped) is deduced from the evolution of the kinetic energy of the particles measured during the flow. The inclination has been varied between 18° and 27° in steps of 1°, and the particle flux has been varied between 300 and 1800 in steps of 300 particles per second. Below a threshold angle, which slightly depends on the particle flux (19° for particle fluxes less than 1000 particles per second), the flows are not steady state and stop. A decrease of the inclination by 3° is enough to stop the flow. This sensitivity to the inclination is consistent with the model describing the influence of the walls at the end of §2.2.2. For angles higher than this threshold angle, flows are collisional in their upper region and dense close to the rough bed, where the solid fraction is higher than 0.6. Moreover, we observe that the bead bed generates a certain local order (structuration in layers) in the first layers (Azanza 1998). In this dense region, the assumptions of the kinetic theory (binary collisions, molecular chaos) may be inappropriate. For angles greater than 21°, the flows are fully collisional and the dense lower area disappears. They become very rapid and continuously accelerated for angles greater than 25°. The same regimes are observed for flows on the jagged bed, but the threshold angle increases from 19° to 23°.

The solid fraction, velocity and granular temperature profiles have special features in the collisional regime (figure 6). The solid fraction decrease is quite linear. The mean transverse velocity (along Oy) is zero. The mean longitudinal velocity (along Ox) increases with height with a non-dimensional gradient about 1. At the bead bed, the slip velocity is rather low. The agitation due to the numerous collisions generates granular temperature. The granular temperature increases as a function of the height. The order of magnitude of the fluctuating velocity, given by its square root, is significant with respect to the mean velocity. Note that these profiles are very different from the case of a simple shear flow.

The main experimental studies of the collisional regime have been performed by Drake (1991), and Ahn *et al.* (1991). In Drake's study, the flow geometry is two-dimensional. Only two quantitative analysis of flows were performed, with a much larger inclination than here, which may have increased extraneous effects (aerodynamic and walls). The main difference between the profiles measured by
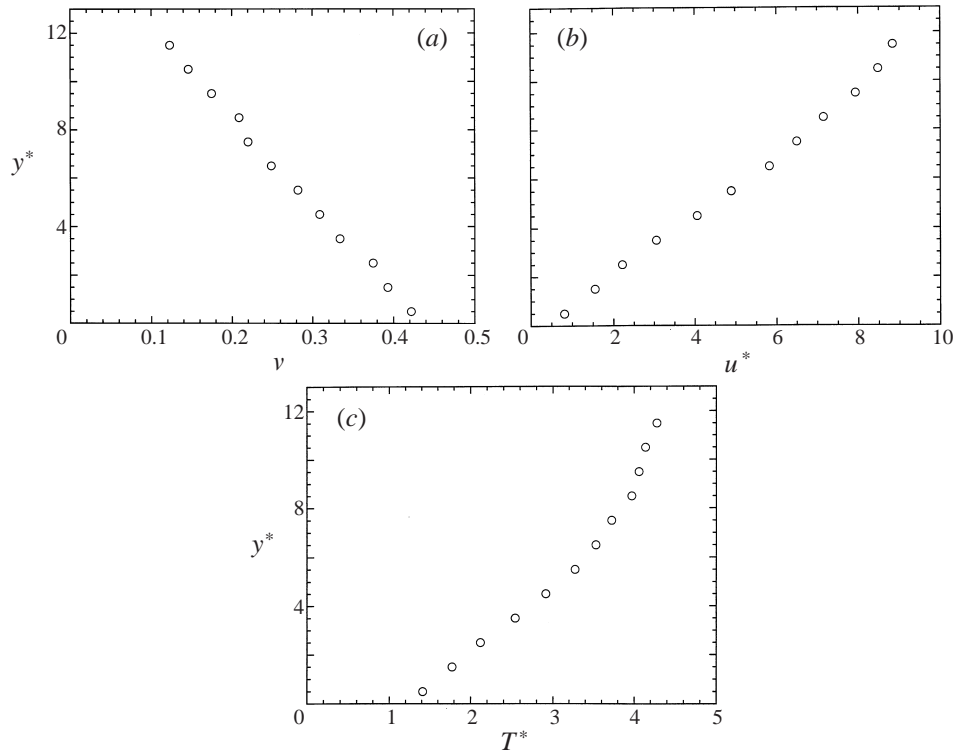
FIGURE 6. Collisional regime: (*a*) profile of solid fraction *v*, (*b*) profile of velocity u^* and (*c*) profile of granular temperature T^* ($\theta = 22°$, $Q \simeq 1100$ particles per second, stuck-bead bed roughness).

Drake and those exhibited below lies in the granular temperature, which is rather constant in Drake's study. The qualitative agreement is better with the study of Ahn *et al.* (1991), even for the granular temperature. However, we must recall that in this case the flow geometry is three-dimensional, and the measurements have been done at the walls.

4.2. *Kinetic theory assumptions – velocity distribution*

Before presenting some results for velocity distribution, let us examine the basic assumptions of the kinetic theory given previously, namely the assumptions of binary collisions, of uncorrelated velocities and of equilibrium state. It is hopped that the first two are globally satisfied (except in the first layers near the bed), even though this is difficult to prove because it is not possible to identify the collision moment with enough precision. But the third assumption can be examined, because we have access to the kinematics of the flows.

4.2.1. *General expression for the velocity distribution*

The velocity distribution function $f(\boldsymbol{r}, \boldsymbol{c})$ is a central quantity in any kinetic theory, on which is based the calculation of the transport coefficients (Reif 1965). A flowing granular material is a non-equilibrium and dissipative medium, showing gradients of solid fraction, velocity and temperature. Let us examine the deviation of this distribution function from the Maxwellian equilibrium case.

This distribution function has been studied previously in vibrated grain experiments (Warr, Huntley & Jacques 1995), and numerical simulations (Knight & Woodcock
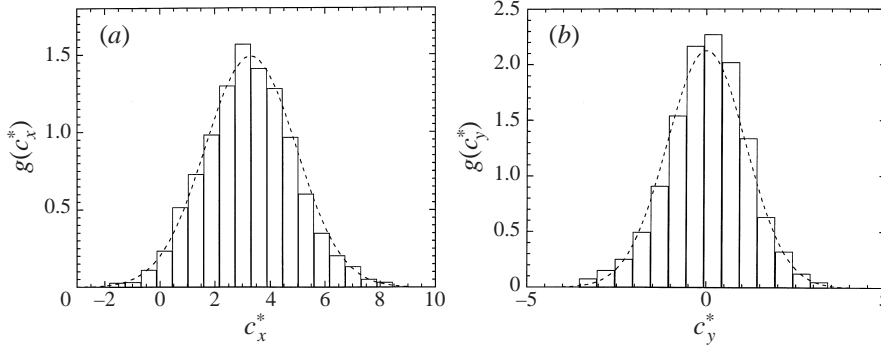
FIGURE 7. Velocity distribution function: (a) longitudinal component $g(c_x^*)$, (b) transverse component $g(c_y^*)$ ($v = 0.39$, $\theta = 21°$, stuck-bead bed roughness). Comparison with the Gaussian distribution.

1996). Figure 7 shows our measurement of the distribution functions for the longitudinal and transverse velocity components at different distances y above the bead bed, inside the layers used to measure the structural and kinematic mean quantities. These distributions are defined as

$$g(y, c_x) = \frac{1}{v(y)} \int f(\mathbf{r}, \mathbf{c}) \, dx \, dc_y, \qquad (4.1)$$

$$g(y, c_y) = \frac{1}{v(y)} \int f(\mathbf{r}, \mathbf{c}) \, dx \, dc_x. \qquad (4.2)$$

At first sight, those distribution functions are nearly Maxwellian, as predicted by the theory. This confirms the observations of Drake (1991) performed in the same solid fraction range. Nevertheless, small deviations from the equilibrium distribution are perceptible. It seems that the distributions are not strictly symmetric and exhibit a peak sharper than a Gaussian one. The distributions measured by Ahn *et al.* (1991) and Warr, Jacques & Huntley (1994) have the same characteristics.

4.2.2. *Anisotropy and asymmetry of the distribution function*

The variance of the velocity distribution measures the granular temperature. We note strong anisotropy between the distributions of the two velocity components. The order of magnitude of this anisotropy has been estimated in flows on various rough beds (figure 8). In spite of the strong scatter of the experimental data, we note that the granular temperature in the direction of the flow is greater than the granular temperature in the transverse direction. The ratio T_y^*/T_x^* is about 0.55 ± 0.1, independent of the value of the solid fraction. It is also independent of the rough bed nature. Drake (1991) also reports that the measured velocity distributions are anisotropic except close to the rough bed. In this case the ratio between the transverse granular temperature and the longitudinal granular temperature amounts to 0.65. Similar anisotropic quasi-Maxwellian distributions have already been observed in numerical simulations of vibrated grains (Knight & Woodcock 1996).

This anisotropy was first revealed by numerical simulations of simple sheared granular media (Campbell & Brennen 1985; Campbell & Gong 1986; Walton & Braun 1986b), on account of a difference between the longitudinal and transverse components of the normal stress, which decreased with the restitution coefficient and solid fraction.

According to Campbell (1989), this anisotropy must be connected to the two modes
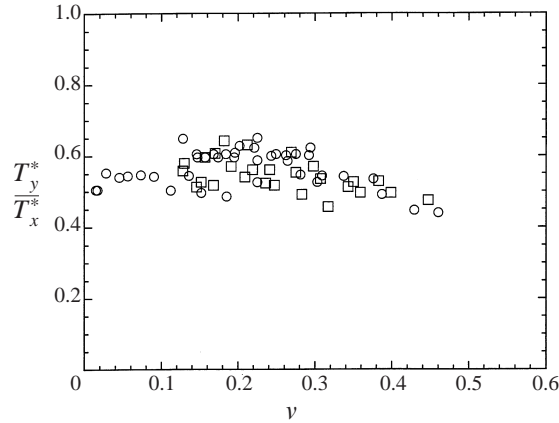
FIGURE 8. Anisotropy of the granular temperature T_y^*/T_x^* as a function of solid fraction v, measured in various flows (stuck-bead bed roughness ($\bigcirc$), jagged profile roughness ($\square$)).
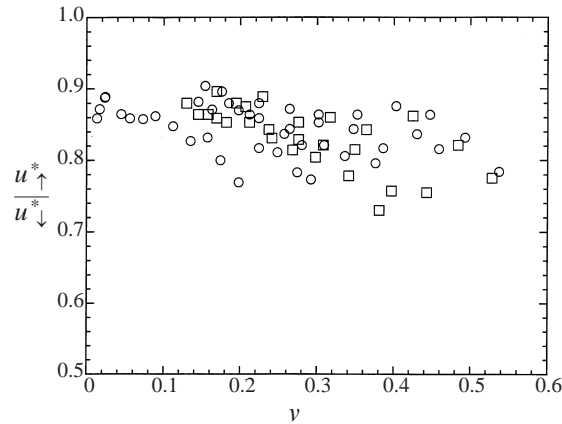
FIGURE 9. Asymmetry of the distribution function $u_\uparrow^*/u_\downarrow^*$ as a function of solid fraction v, measured in various flows and for various y^* (stuck-bead bed roughness ($\bigcirc$), jagged profile roughness ($\square$)).

of granular temperature generation: at high solid fractions, collisions lead to isotropic transfer of momentum; at low solid fractions, the kinetic transport of particles, without collisions, generates a fluctuating velocity perpendicular to the velocity gradient. Unlike the collisional temperature, the kinetic temperature is anisotropic because only the component parallel to the velocity gradient is affected by this mechanism. In contrast with this mechanism, our experimental measurements show that the longitudinal granular temperature is greater than the transverse one, but that the ratio does not depend on the solid fraction. We have not found any satisfactory explanation for this discrepancy, except for the possible influence of the wall.

In order to quantify the asymmetry of the distribution function, which is clear for the transverse velocity, the ratio between the mean longitudinal velocity of the ascending particles ($c_y > 0, \uparrow$) and the descending particles ($c_y < 0, \downarrow$) has been calculated (see Appendix D). The ratio $u_\uparrow/u_\downarrow$ between the mean velocity of ascending particles and the mean velocity of descending particles is shown in figure 9. It is equal to 0.85, roughly constant in terms of the solid fraction, and is independent of the nature of the rough bed. This difference between ascending and descending
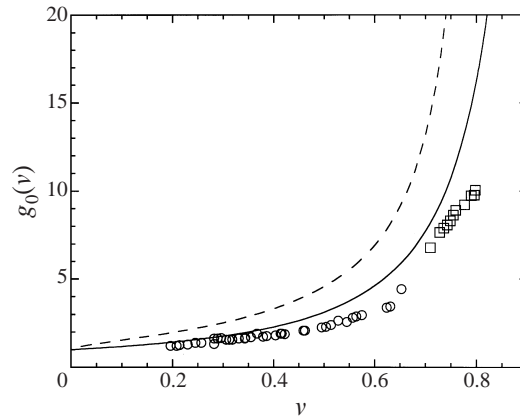
FIGURE 10. Radial distribution function at contact g_0 as a function of solid fraction v. Comparison between experimental data (stuck-bead bed roughness ($\bigcirc$), jagged profile roughness ($\square$)) and theoretical prediction (g_0^{VL} equation (3.8) (——), $g_0^{0.82}$ equation (3.9) (– –)).

particles is obviously due to gravity. Owing to gravity, the particles are accelerated or decelerated between two successive collisions, according to the direction of their velocity. This asymmetry will be calculated in §5.2.

4.3. *Identification of the constitutive law*

Measuring the constitutive law still remains an experimental challenge. In the following, the three elementary functions $f_1(v)$, $f_2(v)$ and $F(v)$ are determined using the solid fraction, velocity and granular temperature profiles measured experimentally. In the subsequent analysis, we do not take into account the experimental points corresponding to a distance less than 3 diameters from the bed, where an organization of the beads in layers is observed.

4.3.1. *Radial distribution function*

Figure 10 shows an experimental determination of the radial distribution function $g_0(v)$, measured according to the calculation given in Appendix C. The experimental data used here come from flows with various characteristics (inclination angles, particle fluxes and roughness of the bed). We have not observed a dependence of the radial distribution function on the velocity gradient which is predicted by some theories (Jenkins & Savage 1983; Campbell & Brennen 1985). The experimental data agree much better with the expression (3.8) given by Verlet & Levesque (1982) than with the expression (3.9). However, there remain discrepancies, especially at high solid fractions, which we suspect to be due to the organization in layers. In the following, the expression (3.8) will be used.

4.3.2. *Function $F(v)$*

The efficiency of the shear in generating granular temperature is measured by the function $F(v)$, which was defined in (3.12):

$$F(v) = \left(\frac{\mathrm{d}u^*}{\mathrm{d}y^*}\right) / \left(\tan\theta \, T^{*1/2}\right). \tag{4.3}$$

Figure 11(*a*) shows the experimental measurement of this function. The points are calculated using the experimental values of solid fraction, granular temperature,
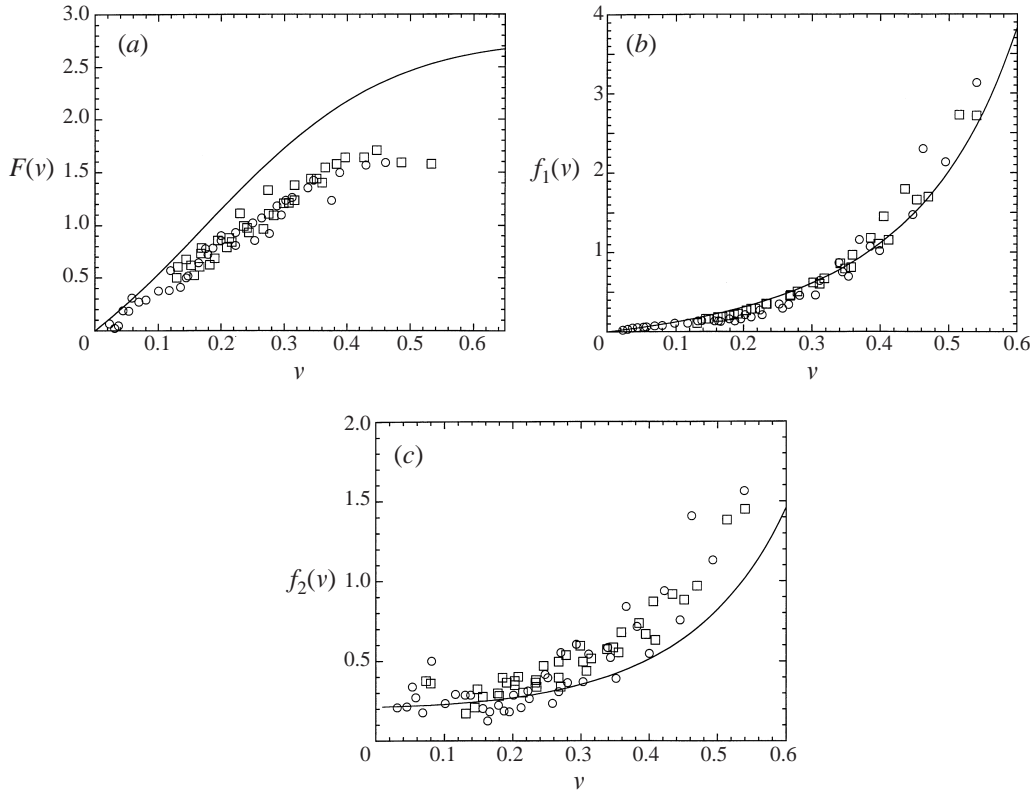
FIGURE 11. (*a*) The function $F(v)$, (*b*) the function $f_1(v)$ and (*c*) the function $f_2(v)$, measured in various flows (stuck-bead bed roughness (○), jagged profile roughness (□)). Comparison with the model of Jenkins & Richman (1985), with $e = 0.95$ (——).

velocity gradient and plane inclination, and come from flows performed at different inclination angles, particle fluxes and roughness of the bed. They are scattered along a reasonably well-defined underlying curve. Therefore, there is a unique relation between the velocity gradient and the square root of granular temperature. Moreover, this relation is not dependent on the nature of the two rough beds. When the solid fraction is low, the granular temperature varies in a linear manner with the velocity gradient, since the flows are highly sheared and the collision rate is low. On the other hand, the function F saturates for a solid fraction higher than 0.4 because the collision rate, which is roughly proportional to the solid fraction, increases whereas the velocity gradient remains constant. The agreement between the theoretical prediction and the experimental data is qualitatively good. For low solid fractions, the discrepancies are within experimental errors, but for higher solid fractions, the theory overestimates the function F by about 30%. The experimental measurement of Ahn *et al.* (1991), even though very noisy, is also lower than the theoretical prediction. The function F has also been measured in numerical simulations of simple shear flows. The agreement with the prediction of the kinetic theory was only qualitative in the study of Campbell & Gong (1986), but quantitatively correct in the study of Walton & Braun (1986*a*).

Since the granular temperature is anisotropic, we have calculated the function F using the experimentally measured granular temperatures T_x, T_y and the average $T = (T_x + T_y)/2$. The high anisotropy leads to a variation by a factor 2. The better

agreement is obtained with T_y, but even in this case the function F remains lower than the theoretical prediction. So we conclude that the discrepancies between the theoretical and experimental Bagnold's relations cannot be explained by the granular temperature anisotropy.

4.3.3. *Pressure and viscous terms*

Using the momentum balance equation projected along the direction normal to the plane (3.11), the function $f_1(v)$ can be calculated once the solid fraction and granular temperature profiles are known. We have used the experimental profiles of solid fraction and granular temperature, in flows at different inclination angles, particle fluxes and roughness of the bed. However, we have made the following simplifying assumptions: in the collisional region, the solid fraction and granular temperature gradients have been considered constant. In the dilute kinetic region, as will be described in § 5.1, the solid fraction was supposed to vary exponentially and the granular temperature to be constant. We have also assumed that the function f_1 vanishes when the solid fraction tends to 0. The function f_1 could then be calculated by solving the differential equation (3.11), and is shown in figure 11(*b*). Like F, the function f_1 does not depend on the nature of the rough bed. Agreement with the function f_1 estimated by Jenkins & Richman (1985) is very good, except at high solid fraction. The pressure term (and not the elementary function f_1) has also been measured in the numerical simulations of simple shear flows by Walton & Braun (1986*a*), and the agreement with the prediction of the kinetic theory was quantitatively correct.

The function f_2 can be calculated, once the functions f_1 and F are known, using the relation $F(v) = f_1/f_2$, and it is shown in figure 11(*c*). It shows the same discrepancy with the theoretical curve as the function F. This discrepancy may be due to the friction between particles during the collisions which is not taken into account by the theory. The numerical simulations of Walton & Braun (1986*b*), which included the rotation of the particles, showed that the viscosity of a simply sheared granular medium increases with the friction coefficient of the particles, when the solid fraction is greater than 0.2. Moreover, they noticed that the pressure is less affected by the friction coefficient, as observed here.

The dependence on solid fraction of the pressure and viscosity, as predicted by the kinetic theory of Jenkins & Richman (1985), has been measured experimentally. The agreement is good for the pressure term, but the viscosity coefficient is smaller, possibly because of the effects generated by the friction between particles during the collisions. Three other functions, f_3, f_4 and f_5, are necessary to quantify a collisional granular flow. It may be shown that the contribution associated with f_4 always remain very small (Adda 1996). The two other functions appear together in the energy equation (3.3), so that it is not possible to identify them separately in the inclined plane geometry. Apart from numerical simulations, we propose the following experiments to measure the functions f_3 and f_5. First, the rate of energy dissipation could be measured directly in a simple plane shear flow geometry where the granular temperature is constant. Then the flux of fluctuation kinetic energy could be measured in a vibrated grains experiment, where the average velocity is nil.

4.4. *Comparison between experimental and theoretical profiles*

We now compare profiles from experiment and theory directly. The theoretical profiles are obtained by solving the system (3.11)–(3.13). This system is first solved by determining v and T^* using (3.11) and (3.13) and then calculating u^* by integrating
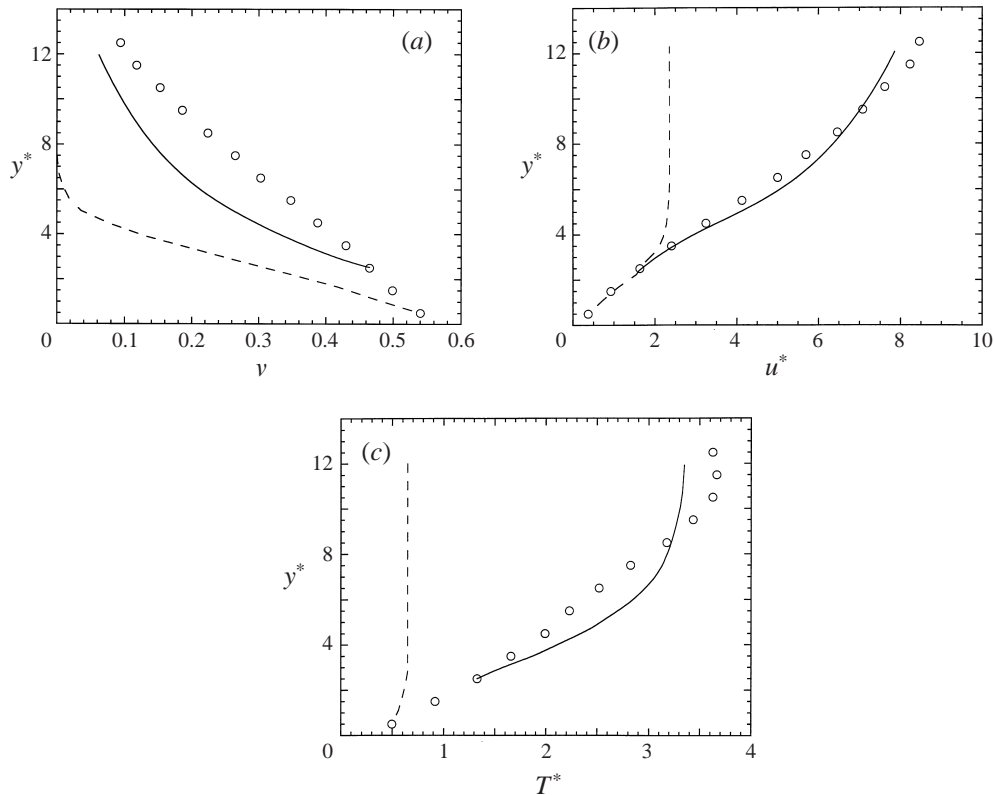
FIGURE 12. Collisional regime: (*a*) profile of solid fraction *v*, (*b*) profile of velocity u^*, (*c*) profile of granular temperature T^*. Comparison between experimental measurements (○) and theoretical predictions ($\theta = 21°$, $e = 0.95$), integrating the equations from the bed (— —), or from a height of two diameters (——).

(3.12). The method developed by Ahn *et al.* (1992) has been used. Equations (3.11) and (3.13) are solved by a fourth-order Runge–Kutta method and a shooting method on the derivative of the granular temperature at the bed. Four boundary conditions are needed: we fix the values of the solid fraction, mean velocity and granular temperature, taking experimental values measured at the bed. The derivative of granular temperature is forced to vanish at infinity, which ensures the nullity of the stresses and the flux of fluctuation kinetic energy at the free surface. This last condition will be justified in § 5.1. We stress that the two parameters in the model (the restitution coefficient *e* and the radial distribution function at contact $g_0(v)$) are determined experimentally. The sensitivity of the numerical solutions to these two quantities has been studied and shown to be small small (Adda 1996).

Figure 12 shows a typical comparison between the experimental and the theoretical profiles of solid fraction, mean velocity and granular temperature, for an inclination of 21° and a stuck-bead bed. Consider first the theoretical solutions obtained when integrating the equations from the bottom of the bed. The theoretical profiles differ a great deal from the experimental data. The main discrepancy lies in the granular temperature: the theoretical profile is almost constant whereas the experimental profile increases linearly and saturates near the surface. The theoretical solid fraction profile is also very different from the experimental profile, which is substantially

underestimated. However, as expected from the measurement of the function $F(v)$, the value of the velocity gradient close to the bead bed has the correct order of magnitude. Nevertheless, the theoretical velocity becomes constant for a height that is far too low. These remarks remain true for comparisons performed at other inclination angles.

On the basis of these observations, the system (3.11)–(3.13) may be questioned. In order to identify the origin of the discrepancy, a series of tests was performed.

First of all, the experimental expression for f_2 was used in place of the theoretical expression. The effect of this change is almost invisible on the solid fraction and the granular temperature profiles, and it remains very weak on the velocity profiles, where the viscosity is proportional to f_2. So the observed discrepancies between the experimental and theoretical data do not come from the function f_2, and in the following, the theoretical expression for the function f_2 will be used.

A second test was performed. We suspect that the kinetic theory becomes invalid near the bead bed where the structuring of the particles may contradict the assumptions of the theory. When integrating the equations from a height of 2 diameters, the theoretical profiles are very different and the comparison with the experimental data is much better. The order of magnitude of the solid fraction, mean velocity and granular temperature is now satisfactory. This shows that the organization of the grains near the rough bed has a considerable influence on the whole flow. This confirms the inadequacy of the theory near the bed roughness.

However the solid fraction and granular temperature gradients still remain too high. The solid fraction gradient is given by (3.11). Since the function f_1 is in excellent agreement with its experimental estimation, we suspect that the discrepancy comes from the granular temperature gradient itself, which is given by the energy equation (3.13). The shear work term should be correct because only the function f_2 occurs. On the other hand, the flux of fluctuation kinetic energy and the rate of energy dissipation may be suspected, but since the functions f_3 and f_5 have not been identified, it is not possible to conclude if the difference comes from the energy equation (3.13). In the future, it would be interesting to study two influences which are not taken into account here : the friction coefficient (particle rotation and dissipation) and the correlations of the velocities.

5. Kinetic regime

As described in §3 the kinetic theory distinguishes the kinetic contribution, which takes the transfer of momentum and fluctuating kinetic energy between two collisions into account, and which dominates the collisional contribution for low solid fraction. In a two-dimensional geometry, the transition occurs at a solid fraction of about 0.29 (Walton & Braun 1986*b*; Campbell & Gong 1986). This value is also obtained by Jenkins & Hanes (1993) from a momentum balance taken in the transition region between the collisional and kinetic regimes. Another estimation is a solid fraction of about 0.2, a value for which the mean distance between the particles is equal to 1 diameter.

In our experiment, we are not able to distinguish the kinetic and collisional contributions. However, as shown in figure 13, it is possible to distinguish two regions in the profiles. In the lower collisional region, the quantities are roughly linear, as has been shown before. Above a height of about 8 diameters, the solid fraction no longer decreases in a linear manner, and the velocity and the granular temperature tend to saturate at a maximum value at the top of the flow. The transition between these two regions usually occurs at a solid fraction of about 0.15, a lower value than
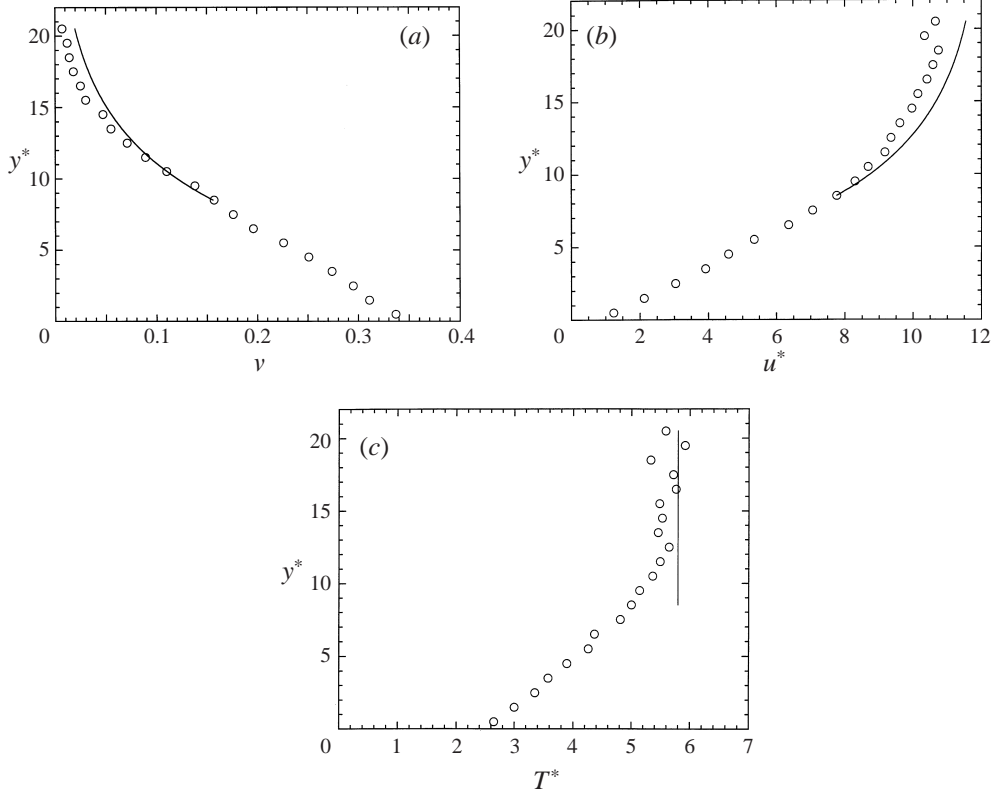
FIGURE 13. Kinetic regime: (*a*) profile of solid fraction v, (*b*) profile of velocity u^*, (*c*) profile of granular temperature T^*. Comparison between experimental measurements ($\bigcirc$) and theoretical predictions (———). ($\theta = 23°$, $Q \simeq 1100$ particles per second, $e = 0.95$).

the previous estimation. We think that the higher region corresponds to true ballistic trajectories, that is to say the dilute kinetic regime.

The study of this regime is necessary to define realistic boundary conditions at the surface of the flows. Because of the very low solid fraction in this regime, the number of images on which the average is calculated has been increased to improve the statistics. Note that the boundary conditions which have been used before to solve the balance equations of the kinetic theory, and which assume that the derivative of the granular temperature vanishes at the top of the flow, are thus realistic with regard to the experimental results.

5.1. *Comparison of experiment and theory*

We now compare the experimental profiles with the theoretical profiles in the kinetic regime. In order to obtain analytical solutions, we take the asymptotic form of the balance equation, when the solid fraction tends to zero. In this case, the three balance equations (3.11)–(3.13) become (with $e \simeq 1$)

$$\frac{\mathrm{d}v}{\mathrm{d}y^*} = -\frac{v}{T^*}\left(1 + \frac{\mathrm{d}T^*}{\mathrm{d}y^*}\right), \tag{5.1}$$

$$\frac{\mathrm{d}u^*}{\mathrm{d}y^*} = \frac{8}{\pi^{1/2}}\, v\, T^{*1/2}\, \tan\theta, \tag{5.2}$$
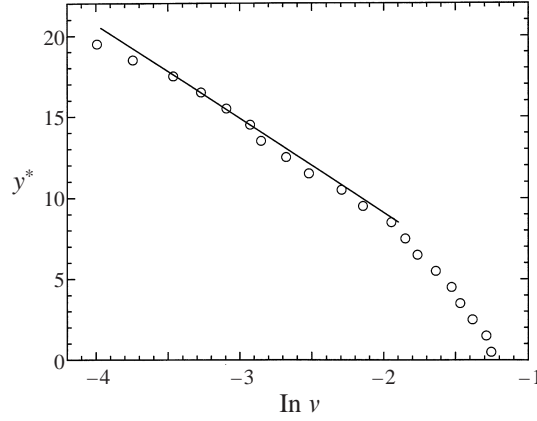
FIGURE 14. Exponential decrease of the solid fraction v in the dilute kinetic zone. ($\theta = 23°$, $Q \simeq 1100$ particles per second).

$$\frac{\mathrm{d}^2 T^*}{\mathrm{d}y^{*2}} = -\frac{1}{2T^*}\left(\frac{\mathrm{d}T^*}{\mathrm{d}y^*}\right)^2. \tag{5.3}$$

Equation (5.3) has two solutions

$$T^* = (A\,y^* + B)^{2/3}, \tag{5.4}$$

$$T^* = T_0^*. \tag{5.5}$$

Only the second solution is acceptable because the granular temperature cannot diverge at the free surface. The solid fraction and velocity are then deduced

$$v^* = v_0 \exp\left(-\frac{y^* - y_0^*}{T_0^*}\right), \tag{5.6}$$

$$u^* = u_0^* + \frac{8}{\pi^{1/2}}\,v_0\,T_0^{*\,3/2}\,\tan\theta\left(1 - \exp\left(-\frac{y^* - y_0^*}{T_0^*}\right)\right). \tag{5.7}$$

Figure 13 compares the theoretical profiles (5.5)–(5.7) with the experimental profiles. Figure 14 shows that the solid fraction variation is exponential near the top of the flow. The granular temperature T_0^* is deduced from logarithmic plotting of the solid fraction profile as a function of the height. It reaches 5.8, a value which agrees well with the measured granular temperature. Also, the comparison between the solid fraction and velocity profiles seems correct, even in a quantitative way. The asymptotic form of the kinetic theory therefore describes well the dilute region at the top of the flows.

However, the kinetic theory which has been considered in the previous comparison postulates that the velocity distribution is isotropic and symmetrical. This is not the case in this region of the flow. This anisotropy and asymmetry are also noticeable on the velocity and granular temperature profiles. Figure 15 shows that the velocity of descending particles ($\downarrow$) is higher than the velocity of ascending particles ($\uparrow$). Also, the granular temperature along the flow direction is higher than in the direction normal to the rough bed. Possible explanations of this anisotropy have been given before. For a very dilute granular medium, the theory of Jenkins & Richman (1988) predicts a difference between the components of the normal stress, but the theoretical value (0.9) is much larger than the experimental one (0.55).
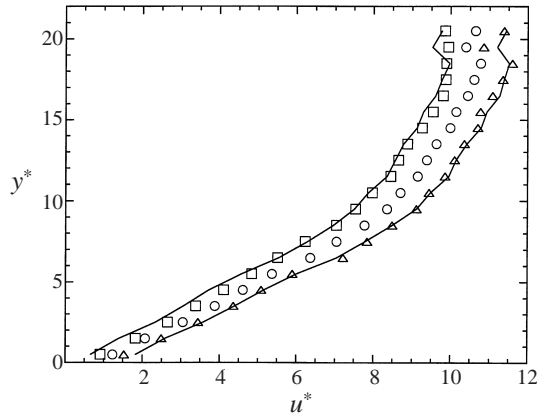
FIGURE 15. Velocity profile for ascending ($\square$), downward ($\triangle$) particles, and with no distinction ($\bigcirc$) ($\theta = 23°$, $Q \simeq 1100$ particles per second). Comparison with a simple ballistic model (——).

5.2. *Estimation of the asymmetry*

A simple model has been developed to estimate the order of magnitude of the asymmetry. We consider a granular flow, which is mainly collisional below the height y_0 and ballistic above. At the transition height y_0, some of the particles are thrown out by the collisions at the top. Then they follow a parabolic trajectory, without any collision, and go back to the collisional region at the altitude y_0.

Following these assumptions, the difference between the mean longitudinal velocities of the descending particles $u_\downarrow^*$ and the ascending particles $u_\uparrow^*$ is calculated in Appendix D

$$u_\downarrow^* - u_\uparrow^* = 2 \tan \theta \, (2 \, T_y^*/\pi)^{1/2}. \tag{5.8}$$

The asymmetry of the longitudinal velocity thus depends on the transverse granular temperature. The order of magnitude of this prediction agrees well with the experimental measurement (figure 15). The fully ballistic model gives a good order of magnitude of the velocity asymmetry in the kinetic region. Surprisingly, this model holds for high solid fraction whereas the assumptions are no longer justified.

6. Conclusion

We have presented an experimental study of the flow of a slightly inelastic granular material down a rough inclined plane. The two-dimensional geometry of the channel and the double flash lighting method allow detailed and complete measurement of the kinematics and structure of the flows. Aerodynamic and electrostatic effects have been shown to be small and the influence of the walls has been estimated. We have determined the range of inclination and particle flux for which the flows are stationary and uniform. These flows are collisional, with a certain local order in the first dense layers near the bed, and very dilute at the free surface. The characteristic profiles of solid fraction, mean velocity and granular temperature have been measured.

These experimental results have been compared with the predictions of a kinetic theory for monodisperse, slightly inelastic and smooth spheres. Velocity distributions are quasi-Maxwellian. A simple relation between the velocity gradient and the granular temperature has been observed. The dependences on solid fraction of the pressure and viscosity have been measured. The agreement is good for the pressure term, but the

viscosity experimentally measured is slightly larger than the theoretical prediction, possibly because of the friction between beads. The comparison of the profiles indicates that the kinetic theory does not work near the bed, probably because of the organization in layers of the flow. Even inside the collisional region there are significant discrepancies, whose origin remains unclear. A specific study of the dilute kinetic regime has been carried out. The asymptotic solution of the kinetic theory at low solid fractions agrees well with the experimental observations. A fully ballistic model predicts the order of magnitude of the velocity asymmetry.

Even for such a simple system, there remain important questions. On the theoretical side, an estimation of the influence of the friction between grains is required. It is also necessary to take into account the structuring of the granular flow and the velocity correlations which occur near the bed, in order to get a better formulation of the boundary conditions. On the experimental side, it would be helpful to measure the rotation of the particles, the flux of agitation and the rate of energy dissipation inside the flow. It would also be interesting to vary the dissipation at the bed and the friction between grains. These aims are difficult experimental challenges, but should be more easily tackled by numerical simulations. Such a combination of theory, experiment and simulation is necessary for a better understanding of granular flows.

Appendix A. Wall friction force

Between two collisions of grains, the momentum balance of a grain in the flow is

$$m\gamma = m\mathbf{g} + \mathbf{F}_f,$$

where $\mathbf{F}_f$ is the mean friction force exerted by the walls on the grain. This force is related to the average variation of the tangential component of the momentum $\mathbf{p}_t$ generated by the collisions at the wall. It may be expressed as

$$\mathbf{F}_f = \frac{\Delta \mathbf{p}_t}{\tau},$$

with τ the average time between two collisions, given by $\tau = \sigma/v_n$, σ being the extra-spacing between the walls and v_n being the velocity normal to the wall. Let us estimate $\Delta \mathbf{p}_t$ by writing the momentum variation during a collision

$$m(v_n^+ - v_n^-) = P_n,$$
$$m(\mathbf{v}_t^+ - \mathbf{v}_t^-) = \mathbf{P}_t.$$

$\mathbf{v}_t$ is the tangential velocity at the wall, the superscripts $+$ and $-$ respectively denote pre- and post-collision quantities, and P_n and P_t are the normal and tangential impulses. Since σ is much smaller than D, the collisions between the grains and the wall occur at very low incidences. Considering then Newton's law for the normal part of the collision and Coulomb's law for the frictional part:

$$P_n = -m(1 + e_w)v_n^-,$$
$$P_t = \mu_w P_n,$$

with e_w and μ_w the coefficient of normal restitution and friction between the grain and the wall, respectively. The order of magnitude of v_n can be deduced by writing the collision laws between two grains and by assuming that their relative velocity parallel to the wall is equal to the square root of the granular temperature

$$v_n = (1 + e) \frac{\sigma}{D} T^{1/2},$$

e is the coefficient of normal restitution between the grains. The factor σ/D comes from the obliqueness of the collision. If we take the non-dimensional form of the granular temperature $T^* = T/gD$, the expression for the wall friction force is

$$\boldsymbol{F}_f = m(1 + e_w)(1 + e)^2 \mu_w \frac{\sigma}{D} g T^* \boldsymbol{t},$$

where $\boldsymbol{t}$ is the unit vector directed in the opposite direction to the mean velocity of the flow.

Appendix B. Expression for the functions f_i and F_i

Expression for the functions f_i (Jenkins & Richman 1985) are

$$f_1(v) = v + 2rv^2 g_0(v),$$

$$f_2(v) = \frac{\pi^{1/2}}{4(5 - 3r)} \left[\frac{1}{g_0(v)} + r(3r - 1)v + \frac{r}{\pi} \left[3\pi r^2 - 2(\pi + 6) + 20 \right] v^2 g_0(v) \right],$$

$$f_3(v) = \frac{\pi^{1/2}}{r(17 - 15r)} \left[\frac{1}{g_0(v)} + 3r \left(2r^2 - \tfrac{3}{2}r + \tfrac{1}{2} \right) v \right.$$
$$\left. + r^2 \left[9r^2 - \left(\frac{30}{\pi} + \frac{27}{4} \right) r + \frac{34}{\pi} \right] v^2 g_0(v) \right],$$

$$f_4(v) = \frac{3\pi^{1/2}(2r - 1)(r - 1)}{2(17 - 15r)} \left[\frac{1}{v g_0(v)} + \frac{3r}{2} \right] \frac{\mathrm{d}}{\mathrm{d}v} \left(v^2 g_0(v) \right),$$

$$f_5(v) = \frac{16r(1 - r)}{\pi^{1/2}} v^2 g_0(v),$$

with $r = (1 + e)/2$.

Expression for the functions F_i are

$$F_1(v) = \frac{1}{f_1'^2 (f_1 f_4 - f_1' f_3)},$$

$$F_2(v) = f_1'^3 \left(\frac{f_1^2}{f_2} \tan^2 \theta - f_5 \right),$$

$$F_3(v) = \tfrac{1}{2} f_1'^3 f_3 - f_1 f_1'^2 f_3' + \tfrac{1}{2} f_1 f_1'^2 f_4 + f_1^2 f_1' f_4' - f_1^2 f_1'' f_4,$$

$$F_4(v) = f_1 f_1' f_4 + (2f_1 f_1' f_4' - 2f_1 f_1'' f_4 - f_1'^2 f_3' + \tfrac{1}{2} f_1'^2 f_4) v,$$

$$F_5(v) = f_1' f_4 v + (f_1' f_4' - f_1'' f_4) v^2,$$

with $f_i' = \mathrm{d}f_i/\mathrm{d}v$.

Appendix C. Determination of the radial distribution function

We consider the flow of N spheres or disks restricted to a plane (position r_i, diameter D, area S_p). The definition of the pair correlation function is

$$g(r_1, r_2) = \frac{n^{(2)}(r_1, r_2)}{n(r_1)\, n(r_2)},$$

where $n(r)$ is the number density whose expression is

$$n(r) = \sum_{i=1}^{N} \delta(r - r_i).$$

The density $n^{(2)}$ is defined as

$$n^{(2)}(r_1, r_2) = \sum_{i,j} \delta(r_1 - r_i)\, \delta(r_{12} - r_{ij}),$$

with $r_{12} = r_1 - r_2$ and $r_{ij} = r_i - r_j$. $n^{(2)}(r_1, r_2) \neq n(r_1)n(r_2)$ because of the correlation of positions of the particles.

Definition of the radial distribution function in the non-uniform case

We consider the case where the flow is uniform in the direction x (over a length L) but non-uniform in the direction y. The expression for the number density is

$$n(r) = \frac{1}{L} \sum_{i} \delta(y - y_i) = \frac{1}{L} n(y)$$

and

$$n^{(2)}(y_1, r_2) = \frac{1}{L} \sum_{i,j} \delta(y - y_i)\, \delta(r_{12} - r_{ij}).$$

The radial distribution function $g(y, r)$ will then depend on the position y. Using the polar coordinates (α, r) where $r_\alpha = r\, n_\alpha$, we calculate the average over the angle α,

$$g(y, r) = \frac{L}{n(y)} \sum_{i=1}^{N} \delta(y - y_i) \frac{1}{2\pi} \int_0^{2\pi} \frac{\sum_j \delta(r_\alpha - r_{ij})}{n(y + r \sin \alpha)}\, d\alpha.$$

We introduce the number of particles $dN_i(r, \alpha)$ around a particle i in the polar differential surface element $r\, dr\, d\alpha$

$$dN_i(r, \alpha) = \sum_j \delta(r_\alpha - r_{ij})\, r\, dr\, d\alpha,$$

so that

$$g(y, r)\, dr = \frac{L}{2\pi r n(y)} \sum_{i=1}^{N} \delta(y - y_i) \int_0^{2\pi} \frac{dN_i(r, \alpha)}{n(y + r \sin \alpha)}.$$

We now define the radial distribution function g_ϵ in a thin layer ϵ around y ($[y - \epsilon/2, y + \epsilon/2]$) along the direction x. We define I_ϵ the indicator function of the layer, equal to 1 inside the layer, and 0 outside. Averaging over the width of the layer, the previous expression becomes

$$g_\epsilon(y, r)\, dr = \frac{L}{2\pi r N_\epsilon} \sum_{i=1}^{N} I_\epsilon(y_i) \int_0^{2\pi} \frac{dN_i(r, \alpha)}{n(y + r \sin \alpha)}.$$

$N_\epsilon = n(y)\epsilon$ is the number of particles in the layer ϵ. The number density and the solid fraction are related by

$$n(y) = \frac{L}{S_p} \, v(y).$$

Using the indicator function $I_{[r,r+dr]}$ of the circular shell $[r, r+dr]$

$$\int_0^{2\pi} \frac{dN_i(r, \alpha)}{v(y + r \sin \alpha)} = \sum_{j=1}^{N} \frac{I_{[r,r+dr]}(r_{ij})}{v(y_j)}.$$

The expression for the radial distribution function is then

$$g_\epsilon(y, r) \, dr = \frac{S_p}{2\pi r} \frac{1}{N_\epsilon} \sum_{i=1}^{N} I_\epsilon(y_i) \sum_{j=1}^{N} \frac{I_{[r,r+dr]}(r_{ij})}{v(y_j)}.$$

The value $g_\epsilon(y, D)$, for the height y where the solid fraction is equal to v, gives the radial distribution function at contact $g_0(v)$.

Appendix D. Estimation of the asymmetry from a ballistic model

In the absence of collisions, the single-particle distribution function $f(y, c)$ is conserved along the trajectories, according to Liouville's theorem (Reif 1965). We propose an expression for f which is consistent with this conservation property. Let us consider the flight of a particle in the ballistic region, above y_0. At any height $y > y_0$, the velocity c_y of the particle in the ascending phase ($\uparrow$) is exactly the opposite of its velocity c_y in the descending phase ($\downarrow$). In contrast to the velocity c_x, the horizontal velocity $c_h = c_x + c_y \tan \theta$ is conserved along the motion. This suggests an expression for the distribution function at the altitude y_0 which is valid equally for the ascending and descending particles

$$f(y_0, c) = \frac{v_0}{2\pi(T_h T_y)^{1/2}} \exp\left(-\frac{(c_h - u_h)^2}{2 T_h} - \frac{c_y^2}{2 T_y}\right).$$

T_h and T_y are the granular temperatures connected to the velocity fluctuations in the horizontal direction and in the direction normal to the plane respectively. It is easy to show that this distribution function is the solution of Boltzmann's equation in the absence of collisions. Using the conservation property of the distribution function along the trajectories, we obtain its expression at any altitude $y > y_0$

$$f(y, c) = f(y_0, c) \exp\left(-\frac{g \cos \theta \, (y - y_0)}{T_y}\right). \tag{D 1}$$

Thanks to this expression, we are then able to calculate the mean quantities which characterize the flow. Let us begin with the solid fraction

$$v(y) = \int f(y, c) \, dc = v_0 \exp\left(-\frac{g \cos \theta \, (y - y_0)}{T_y}\right).$$

The profile shape agrees with the solution predicted by the kinetic theory. Note that it is the granular temperature T_y which is involved rather than the granular temperature $T = (T_x + T_y)/2$ as in an isotropic case.

We now calculate the mean velocity of the flow for the ascending and descending particles. The expression for the mean velocity is

$$u_{i\uparrow\downarrow}(y) = \frac{1}{v_{\uparrow\downarrow}(y)} \int_{\uparrow\downarrow} c_i\, f(y,\boldsymbol{c})\, \mathrm{d}\boldsymbol{c},$$

so that

$$u_{y\uparrow\downarrow} = \pm \left(2\,T_y/\pi\right)^{1/2},$$
$$u_{h\uparrow\downarrow} = u_h,$$
$$u_{x\uparrow\downarrow} = u_h \pm \tan\theta \left(2\,T_y/\pi\right)^{1/2}.$$

REFERENCES

ADDA, F. 1996 Numerical study of the kinetic theory for granular flows down an inclined plane. *Tech. Rep.* Laboratoire Central des Ponts et Chaussées.

AHN, H., BRENNEN, C. E. & SABERSKY, R. H. 1991 Measurements of velocity, velocity fluctuation, density, and stresses in chute flows of granular materials. *Trans. ASME* E: *J. Appl. Mech.* **58**, 792–803.

AHN, H., BRENNEN, C. E. & SABERSKY, R. H. 1992 Analysis of fully developed chute flow of granular materials. *Trans. ASME* E: *J. Appl. Mech.* **59**, 109–119.

AZANZA, E. 1998 Two-dimensional granular flows down an inclined plane. PhD thesis, Ecole Nationale des Ponts et Chaussées, Paris.

AZANZA, E., CHEVOIR, F. & MOUCHERONT, P. 1997 Experimental study of rapid granular flows in a two-dimensional channel. In *Powders and Grains 97* (ed. R. P. Behringer & J. T. Jenkins), pp. 455–458. Rotterdam: A. A. Balkema.

BAGNOLD, R. A. 1954 Experiments on a gravity-free dispersion of large solid spheres in a newtonian fluid under shear. *Proc. R. Soc. Lond.* A **225**, 49–63.

BOWDEN, F. P. & TABOR, D. 1950 *The Friction and Lubrication of Solids.* Clarendon.

BROWN, R. L. & RICHARDS, J. C. 1970 *Principles of Powder Mechanics.* Pergamon.

CAMPBELL, C. S. 1986 The effect of microstructure development on the collisional stress tensor in a granular flow. *Acta Mech.* **164**, 107–125.

CAMPBELL, C. S. 1989 The stress tensor for simple shear flows of a granular material. *J. Fluid Mech.* **203**, 449–473.

CAMPBELL, C. S. 1990 Rapid granular flows. *Ann. Rev. Fluid Mech.* **22**, 57–92.

CAMPBELL, C. S. 1993 Boundary interactions for two-dimensional granular flows. Part 1. Flat boundaries, asymmetric stresses and couple stresses. *J. Fluid Mech.* **247**, 111–136.

CAMPBELL, C. S. & BRENNEN, C. E. 1985 Computer simulation of granular shear flows. *J. Fluid Mech.* **151**, 167–188.

CAMPBELL, C. S. & GONG, A. 1986 The stress tensor in a two-dimensional granular shear flow. *J. Fluid Mech.* **164**, 107–125.

DRAKE, T. G. 1991 Granular flow: physical experiments and their implications for microstructural theories. *J. Fluid Mech.* **225**, 121–152.

HANES, D. M., WALTON, O., ZAKIROV, V., LOCURTO, G. & BUCKLIN, R. 1997 Observations and simulations of the flow of nearly-ellipsoidal, inelastic particles down a bumpy incline. In *Powders and Grains 97* (ed. R. P. Behringer & J. T. Jenkins), pp. 459–461. Rotterdam: A. A. Balkema.

ISHIDA, M. & SHIRAI, T. 1979 Velocity distributions in the flow of solid particles in an inclined open channel. *J. Chem. Engng Japan* **12**, 46–50.

JENKINS, J. T. & HANES, D. M. 1993 The balance of momentum and energy at an interface between colliding and freely flying grains in a rapid granular flow. *Phys. Fluids* A **5**, 781–783.

JENKINS, J. T. & RICHMAN, M. W. 1985 Kinetic theory for plane flows of a dense gas of identical, rough, inelastic, circular discs. *Phys. Fluids* **28**, 3485–3494.

JENKINS, J. T. & RICHMAN, M. W. 1988 Plane simple shear of smooth inelastic circular discs: the anisotropy of the second moment in the dilute and dense limits. *J. Fluid Mech.* **192**, 313–328.

JENKINS, J. T. & SAVAGE, S. B. 1983 A theory for the rapid flow of identical, smooth, nearly elastic, spherical particles. *J. Fluid Mech.* **130**, 187–202.

JOHNSON, P. C., NOTT, P. & JACKSON, R. 1990 Frictional-collisional equations of motion for particulate flows and their application to chutes. *J. Fluid Mech.* **210**, 501–535.

KNIGHT, T. A. & WOODCOCK, L. V. 1996 Test of the equipartition principle for granular spheres in a saw-tooth shaker. *J. Phys.* A: *Math. Gen.* **29**, 4365–4387.

LOUGE, M. Y. 1994 Computer simulations of rapid granular flows of spheres interacting with a flat, frictional boundary. *Phys. Fluids* **6**, 2253–2269.

LOWELL, J. & ROSE-INNES, A. C. 1980 Contact electrification. *Adv. Phys.* **29**, 947–1023.

LUN, C. K. K. 1991 Kinetic theory for granular flow of dense, slightly inelastic, slightly rough spheres. *J. Fluid Mech.* **233**, 539–559.

LUN, C. K. K. & BENT, A. A. 1994 Numerical simulation of inelastic frictional spheres in simple shear flow. *J. Fluid Mech.* **258**, 335–353.

LUN, C. K. K., SAVAGE, S. B., JEFFREY, D. J. & CHEPURNIY, N. 1984 Kinetic theories for granular flow: inelastic particles in couette flow and slightly inelastic particles in a general flowfield. *J. Fluid Mech.* **140**, 223–256.

NEDDERMAN, R. M. 1992 *Statics and Kinematics of Granular Materials.* Cambridge University Press.

REIF, F. 1965 *Fundamentals of Statistical and Thermal Physics.* McGraw-Hill.

SAVAGE, S. B. 1979 Gravity flow of cohesionless granular materials in chutes and channels. *J. Fluid Mech.* **92**, 53–96.

SAVAGE, S. B. & DAI, R. 1993 Wall slip velocities, layering and self diffusion. *Mech. Mat.* **16**, 225–238.

SAVAGE, S. B. & JEFFREY, D. J. 1981 The stress tensor in a granular flow at high shear rates. *J. Fluid Mech.* **110**, 255–272.

VERLET, L. & LEVESQUE, D. 1982 Integral equations for classical fluids III. The hard discs system. *Molec. Phys.* **46**, 969–980.

WALTON, O. R. & BRAUN, R. L. 1986a Stress calculations for assemblies of inelastic spheres in uniform shear. *Acta Mech.* **63**, 73–86.

WALTON, O. R. & BRAUN, R. L. 1986b Viscosity and temperature calculations for shearing assemblies of inelastic, frictional discs. *J. Rheol.* **30**, 949–980.

WARR, S., HUNTLEY, M. & JACQUES, T. H. 1995 Fluidization of a two-dimensional granular system: experimental study and scaling behaviour. *Phys. Rev.* E **52**, 5583–5595.

WARR, S., JACQUES, G. & HUNTLEY, J. 1994 Tracking the translational and rotational motion of granular particles – use of high-speed photography and image processing. *Powder Tech.* **81**, 41–56.

ZHANG, Y. & CAMPBELL, C. S. 1992 The interface between fluid-like and solid-like behaviour in two-dimensional granular flows. *J. Fluid Mech.* **237**, 541–568.